The Response of Large-Scale Circulation to Obliquity-Induced Changes in Meridional Heating Gradients

DAMIANOS F. MANTSIS, BENJAMIN R. LINTNER, ANTHONY J. BROCCOLI, AND MICHAEL P. ERB

Rutgers, The State University of New Jersey, New Brunswick, New Jersey

AMY C. CLEMENT

University of Miami, Miami, Florida

HYO-SEOK PARK

School of Earth and Environmental Sciences, Seoul National University, Seoul, South Korea

(Manuscript received 29 August 2013, in final form 11 February 2014)

ABSTRACT

The inter- and intrahemispheric climate responses to a change in obliquity are investigated using the Geophysical Fluid Dynamics Laboratory Climate Model, version 2.1. (GFDL CM2.1). Reduced obliquity causes a weakening of the seasonal insolation contrast between the summer and winter hemispheres and a strengthening of the meridional insolation gradient within the summer hemisphere. The interhemispheric insolation change is associated with weakening of the cross-equatorial Hadley circulation and reduced heat transport from the summer hemisphere to the winter hemisphere, in both the ocean and atmosphere. In contrast, the intrahemispheric insolation change is associated with increased midlatitude summer eddy activity as seen by the increased atmospheric heat transport at those latitudes. Analysis of the zonal mean atmospheric meridional overturning circulation on isentropic surfaces confirms the increase of the midlatitude eddy circulation, which is driven by changes of sensible and latent heat fluxes, as well as changes in the stratification or distribution of entropy. It is suggested that the strengthening of this circulation is associated with an equatorward shift of the ascending branch of the winter Hadley cell.

1. Introduction

Obliquity, or the tilt of Earth's rotational axis, is one of the astronomical parameters controlling the latitudinal distribution of top-of-atmosphere (TOA) incoming solar radiation. The axial tilt fluctuates from 22° to 24.5° with a period of 41 000 yr, and proxy records have documented its effect on past climate, especially from 0.8 to 3.0 million years ago when climate variability appears to have been dominated by obliquity-induced 41 000-yr cycles (Raymo and Nisancioglu 2003; Liu and Herbert 2004; Lawrence et al. 2006). Over the last 800 000 years, the variability of the global climate has been dominated by 100 000-yr cycles (Raymo and Nisancioglu 2003), although proxy evidence indicates that some components of the climate system (i.e., the meridional heat transport) have continued to vary with the frequency of obliquity (Vimeux et al. 1999).

Over the course of the annual cycle, a change in obliquity represents a change in the equatorially symmetric TOA heating contrast between high and low latitudes (Mantsis et al. 2011). However, obliquity-induced changes in the seasonal distribution of the TOA insolation are asymmetric with respect to the equator, and manifest a more complicated meridional structure, with an equator-to-pole (or intrahemispheric) insolation contrast as well as an interhemispheric one (Fig. 1).

Earth's climate response to asymmetric interhemispheric forcing has been the subject of modeling studies involving Northern Hemisphere ice sheets (Chiang and Bitz 2005),

Denotes Open Access content.

Corresponding author address: Damianos F. Mantsis, Department of Environmental Sciences, Rutgers, The State University of New Jersey, 14 College Farm Road, New Brunswick, NJ 08901-8551.
E-mail: dmantsis@envsci.rutgers.edu

DOI: 10.1175/JCLI-D-13-00526.1

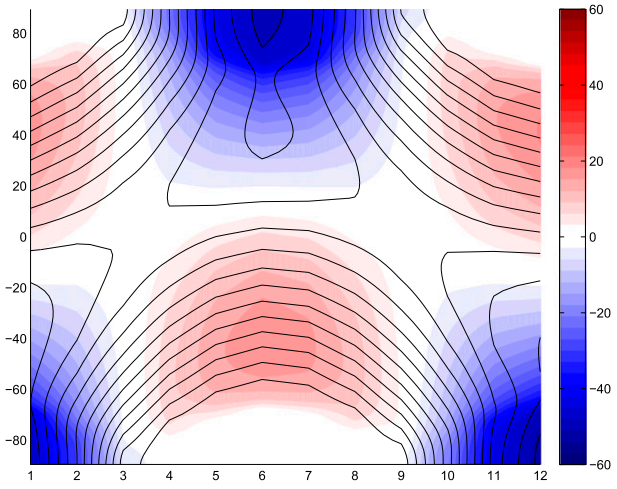

FIG. 1. Seasonal cycle of the TOA insolation (W m^{-2}) climatology (contours) and anomalies (low minus high obliquity) as a function of latitude. Contours represent preindustrial climate.

freshening of the North Atlantic with glacial meltwater (Zhang and Delworth 2005), and greenhouse gases and aerosols (Yoshimori and Broccoli 2008). Other studies (e.g., Broccoli et al. 2006; Kang et al. 2008) have undertaken idealized simulations of the climate response to an anomalous interhemispheric dipole imposed in the surface energy budget. These studies point to reorganization of the tropical circulation in order to balance the hemispherically asymmetric radiative heating by transporting heat from the anomalously warmer to the cooler hemisphere. The Hadley circulation plays a key role in achieving this reorganization: it does so through relative strengthening of the cell in the cooler hemisphere and weakening of the cell in the warmer hemisphere. At the same time the mean latitude of the intertropical convergence zone (ITCZ) migrates toward the warmer hemisphere. Most of these studies have used a slab ocean in which ocean dynamics are absent. However, in the tropics this is a significant limitation since the ocean accounts for a large fraction of the poleward heat transport and even dominates over the atmospheric component close to the equator (Trenberth and Caron 2001). Therefore, in simulations lacking ocean dynamics, the atmospheric circulation alone must balance the asymmetric forcing, which can result in both an amplified Hadley response as well as enhanced poleward heat transport compared to an interactive ocean configuration (Held 2000).

The primary focus of the present study is to develop knowledge of the fundamental physics governing the response of the meridional circulation to obliquity changes. Our analysis uses a fully coupled climate model and focuses on the solstitial seasons during which both interhemispheric and intrahemispheric heating contrasts occur. We diagnose the meridional overturning circulation on dry and moist isentropes to visualize the meridional trajectory of air masses (Held and Schneider 1999; Pauluis et al. 2008, 2010; Laliberté et al. 2012).

2. Model description and experimental design

We use the Geophysical Fluid Dynamics Laboratory (GFDL) coupled atmosphere–ocean general circulation model [Climate Model, version 2.1 (CM2.1); Delworth et al. 2006]. The horizontal resolution of the atmosphere and land models in the version of CM2.1 used here is 2.5° longitude by 2° latitude, and the atmospheric model has 24 levels in the vertical. The resolution of the ocean model at middle and high latitudes is 1° × 1°, but with increasing meridional resolution equatorward of 30° latitude such that it is 1/3° at the equator. There are 50 vertical levels in the ocean, with 22 levels of 10-m thickness each in the top 220 m. The ocean component uses a true freshwater-flux boundary condition when precipitation and runoff enter the ocean. Further details regarding this model formulation can be found in Mantsis et al. (2011).

We conduct two idealized simulations, one with high obliquity (24.480°) and one with low obliquity (22.079°), with all other forcing parameters (i.e., solar irradiance, greenhouse gas concentrations, and surface boundary conditions) set to preindustrial (1860) conditions. The obliquity values used in this study reflect the extremes of obliquity variations during the last 600 kyr of the Quaternary (Berger and Loutre 1991). Both the high and low obliquity simulations are initialized from year 1000 of a preindustrial run of CM2.1. Each of these simulations is run for another 600 years, which is sufficient for the surface and upper ocean to approach equilibrium (Hewitt et al. 1998). The study analyzes the last 100 years of December–February (DJF) and June–August (JJA) seasonal means. In what follows, differences or changes refer to the low minus high obliquity scenarios, unless otherwise stated.

3. Results

a. Overview of the TOA forcing

A change in obliquity does not, by itself, alter the annual global mean insolation received by Earth, but it does affect the seasonal and meridional distribution of TOA insolation (Fig. 1). Lower obliquity increases the insolation throughout the year close to the equator (from 10°S to 10°N), while higher latitudes experience a general increase in winter insolation and a decrease in summer insolation. The TOA insolation change at high latitudes

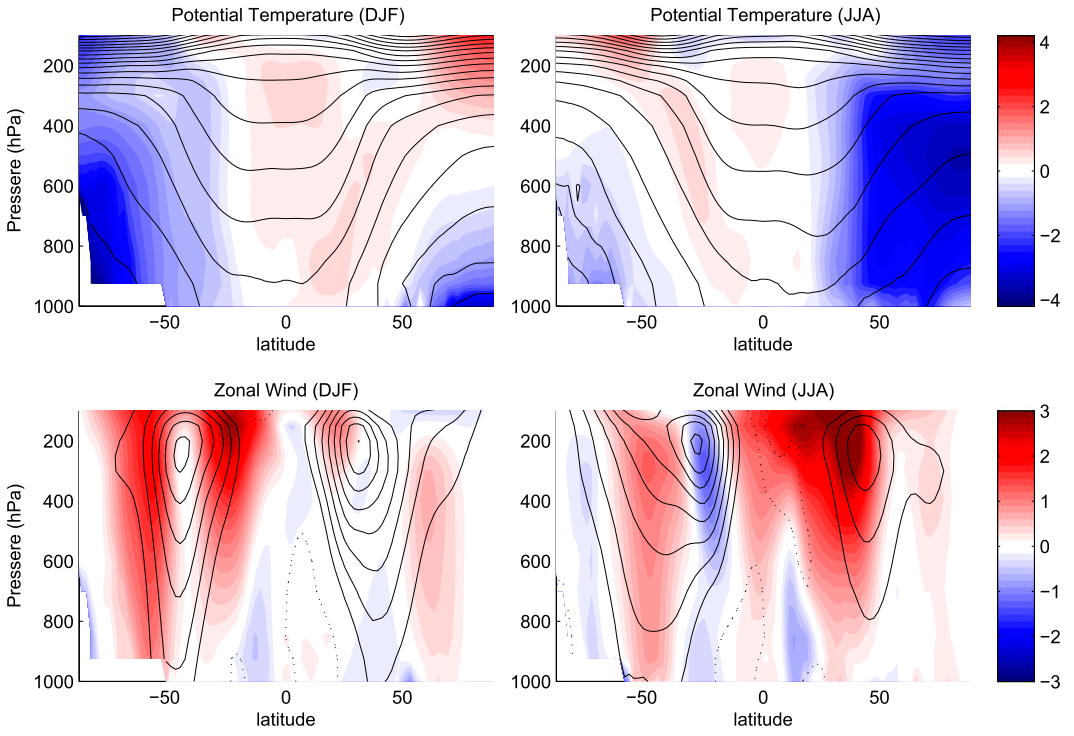

FIG. 2. Climatological conditions (contours) and low minus high anomalies (colors) for (top) potential temperature (K) and (bottom) zonal wind ($m\,s^{-1}$) for DJF and JJA.

associated with low obliquity conditions results in weakening of the insolation seasonal cycle in both hemispheres. The winter increase in insolation extends to the equator, and has maximum values in the midlatitudes. On the other hand, the reduced summer TOA insolation is much greater, compared to the winter increase, with maximum anomalies occurring at the poles. These changes impact the meridional insolation gradient through 1) weakening of the seasonal interhemispheric insolation difference and 2) strengthening of the meridional insolation gradient in the midlatitudes of the summer hemisphere. The distinction between changes in the interhemispheric and intrahemispheric gradients is important because the first one has a substantial impact in the tropics and can affect the heat exchange between the two hemispheres via the Hadley circulation, while the second influences the midlatitudes of the summer hemisphere and can affect the eddy heat transport from low to high latitudes.

b. *Thermal wind and baroclinicity*

Obliquity-induced changes in TOA insolation directly impact the meridional and vertical structure of the zonal mean temperature (Fig. 2, top) as simulated by CM2.1. The largest anomaly corresponds to cooling in the summer hemisphere, as TOA insolation weakens there. This cooling spans the entire hemisphere outside of the tropics and is more pronounced closer to the poles. The winter hemisphere at middle and high latitudes experiences some warming in the upper levels of the atmosphere. In contrast, the lower troposphere and midtroposphere experience some cooling, despite the positive forcing in the midlatitudes. This cooling is strongest at the surface and occurs closer to the poles, even though the forcing is almost zero there. In fact, such cooling appears to stem from the thermal lag of the upper ocean, which experiences reduced heat uptake during summer when the radiative forcing perturbation is strongly negative. In contrast, the tropics experience a slight warming throughout the year because of the positive year-round TOA forcing. The overall result is an increase in the meridional temperature gradient in the summer hemisphere and a smaller increase in the winter hemisphere. As we see below, both hemispheres' gradients are important for the strength of the zonal circulation.

Of course, climate feedbacks modulate the impact of obliquity-induced TOA forcing on temperature and consequently the zonal circulation (Mantsis et al. 2011; Erb et al. 2013). For example, even though the TOA forcing to lower obliquity is identical for both hemispheres during local summer, the cooling is greater in the NH midlatitudes. This is likely related to the combined effects of

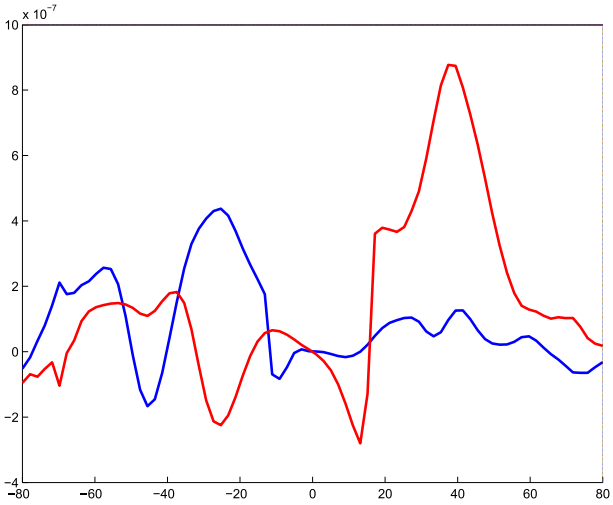

FIG. 3. Eady growth rate (s^{-1}) change (low minus high obliquity) as a function of latitude for DJF (blue) and JJA (red).

positive water vapor, lapse rate, and cloud feedbacks that are generally stronger in the NH midlatitudes compared to the SH midlatitudes (Erb et al. 2013).

The tropical warming also alters the tropospheric dry static stability, which slightly increases in the ascending branch of the Hadley circulation. This is because free tropospheric temperatures are close to moist adiabatic, and thus the change in dry static stability ($\partial\theta/\partial p$) averaged over the troposphere is proportional to the boundary layer moisture, which increases with surface temperature according to the Clausius–Clapeyron relationship (Lu et al. 2008).

Also, the largest changes in the zonal mean wind are located in the summer hemisphere, exactly where the largest changes in the meridional temperature gradient take place (Fig. 2, bottom), in accordance with thermal wind balance. The most notable aspect of the zonal wind response is the equatorward expansion of the subtropical jet, which is also associated with increasing vertical zonal wind shear ($\partial u/\partial z$) in that region. Changes in baroclinic activity are also expected to occur in the summer hemisphere subtropics to midlatitudes (30°–50° latitude). According to Phillips (1954), baroclinic instability is proportional to the lower troposphere (850–500 hPa) vertical wind shear ($\partial u/\partial z$), but inversely proportional to the lower troposphere dry static stability ($\partial\theta/\partial p$). Therefore, we anticipate increasing baroclinic activity in the summer hemisphere under low obliquity conditions, as the wind shear increases and the static stability remains relatively unchanged at those latitudes. Calculation of the Eady growth rate, as defined in Simmonds and Lim (2009), also confirms that the eddy activity increases in the summer hemisphere (Fig. 3).

c. *Meridional overturning circulation and poleward heat transport*

The winter hemisphere Hadley cell simulated by CM2.1 dominates the tropical overturning circulation as the zonal mean Eulerian streamfunction shows (Fig. 4). As obliquity is reduced, the winter Hadley cell weakens (Fig. 4) in both hemispheres [i.e., 4% for the northern cell (DJF) and 6% for the southern cell (JJA)]. According to Dima and Wallace (2003), the seasonality of the Hadley circulation can be decomposed into two leading modes: an annual mode symmetric about the equator, which is associated with the equator-to-pole heating gradient, and a seasonally varying asymmetric solstitial mode, which is a deviation from the annual one. The solstitial mode (winter cell) is related to the interhemispheric heating contrast and is responsible for the net transport of moist static energy from the summer to the winter hemisphere. Thus, any changes in the cross-equatorial overturning circulation have to be explained by changes in the interhemispheric heating contrast.

As obliquity decreases, the annual pole-to-equator heating gradient strengthens and the annual mode strengthens (Mantsis et al. 2011). On the other hand, during the solstices the interhemispheric heating contrast decreases, meaning that the winter Hadley circulation and the associated cross-equatorial heat transport from the warm to the cold hemisphere must weaken (Fig. 5). Indeed, the cross-equatorial atmospheric heat transport (averaged between 15°S and 15°N) weakens by 0.25 PW (11%) during DJF and 0.22 PW (8%) during JJA. This is consistent with the fact that the winter Hadley cell is driven by the energetic and radiative balance (Held and Hou 1980; Schneider 2006; Kang and Lu 2012). Further, the ascending branch of the winter Hadley cell and the associated ITCZ shift toward the equator (by ~1°). A displacement of the ITCZ toward the anomalously warm hemisphere has been shown to be consistent with reduced cross-equatorial heat transport (Zhang and Delworth 2005; Yoshimori and Broccoli 2008; Kang et al. 2008; Mantsis and Clement 2009).

These results demonstrate that the extent of the winter Hadley cell diminishes in favor of the summer cell, which strengthens. In contrast to the winter Hadley cell, the (weaker) summer cell is driven by baroclinic eddies to a much greater extent than energetic and radiative considerations (Held and Hou 1980; Schneider 2006; Walker and Schneider 2006; Schneider and Bordoni 2008; Bordoni and Schneider 2010; Lu et al. 2008; Kang and Lu 2012). As noted in section 3b, baroclinic instability increases with reduced obliquity, with the summer Hadley cell becoming baroclinically unstable to lower latitudes; therefore its poleward descending branch moves equatorward. This

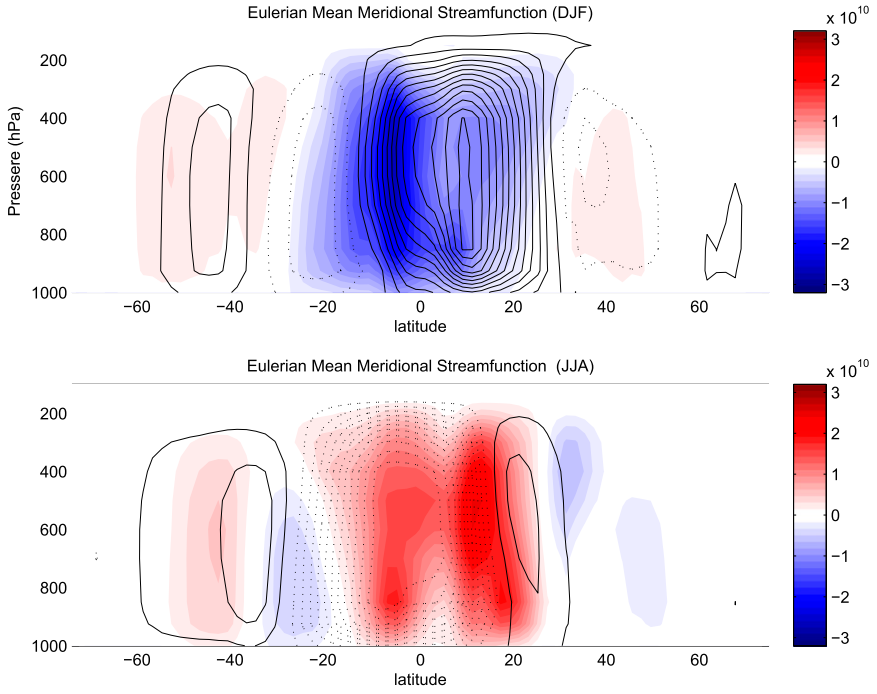

FIG. 4. Climatological conditions (contours) and low minus high anomalies (colors) for the zonal mean Eulerian streamfunction ($kg\,s^{-1}$) for (top) DJF and (bottom) JJA.

behavior is qualitatively consistent with studies on the weakening of the baroclinic instability in the summer subtropics resulting from global warming in which the descending branch of the summer Hadley cell has been found to expand poleward (Lu et al. 2008; Kang and Lu 2012). Of course, the source of the baroclinicity change in the obliquity simulations is the meridional temperature gradient, in contrast to global warming simulations in which it is driven by a change in static stability.

In the midlatitudes, baroclinic eddies dominate the circulation and the poleward heat transport. Under enhanced baroclinicity at low obliquity, the poleward heat transport in the midlatitudes (averaged from 30° to 50°) strengthens by 9% during DJF and by 26% during JJA. We also note that the atmospheric poleward heat transport is reduced in the midlatitudes of the winter hemisphere and is enhanced slightly in the high latitudes of the summer hemisphere, which are both energetically consistent with the seasonal insolation changes at these latitudes.

Thus far, we have focused on the atmospheric response, although the ocean also adjusts to the obliquity forcing. Unlike atmospheric heat transport, ocean heat transport is climatologically maximized in the tropics (Fig. 5, top). As obliquity decreases, the largest changes in the ocean heat transport also occur in the tropics (Fig. 5, bottom). During DJF the cross-equatorial heat transport, averaged between 15°S and 15°N, decreases by 0.27 PW (6%), with the Indo-Pacific basin accounting for most of the decrease, while the Atlantic experiences a small change (not shown). On the other hand, during JJA the reduction is smaller, 0.04 PW (2%). The smaller change during JJA occurs because the southward heat transport strengthens just to the north of the equator, which is offset largely by weakening located on both sides of the equator as discussed below. Again the largest contribution comes from the Indo-Pacific basin, although the Atlantic component dominates from 10° to 17°S. The ratio of atmospheric to oceanic heat transport anomalies, averaged from 15°S to 15°N, is 1:1 during DJF, but is 5:1 during JJA. This indicates that the ocean plays a role in balancing the obliquity-induced changes in radiative heating.

However, given the large heat capacity of the ocean, it is possible that seasonal storage and release of thermal energy may balance part of the obliquity forcing. The question is how much is the heat storage going to contribute in balancing the forcing compared to the heat transport? For a volume of ocean at equilibrium, the heat exchange Q_{NET} between the ocean and the atmosphere needs to be balanced by the ocean heat storage and the heat flux divergence $\nabla \cdot F_o$, which represents the meridional ocean heat transport:

$$\int \left(\rho c_p \frac{\partial \overline{T}}{\partial t} \right) dz + \nabla \cdot F_o = \mathrm{SW}_{\mathrm{surf}} - \mathrm{LW}_{\mathrm{surf}} - \mathrm{LH} - \mathrm{SH} = Q_{\mathrm{NET}}. \quad (1)$$

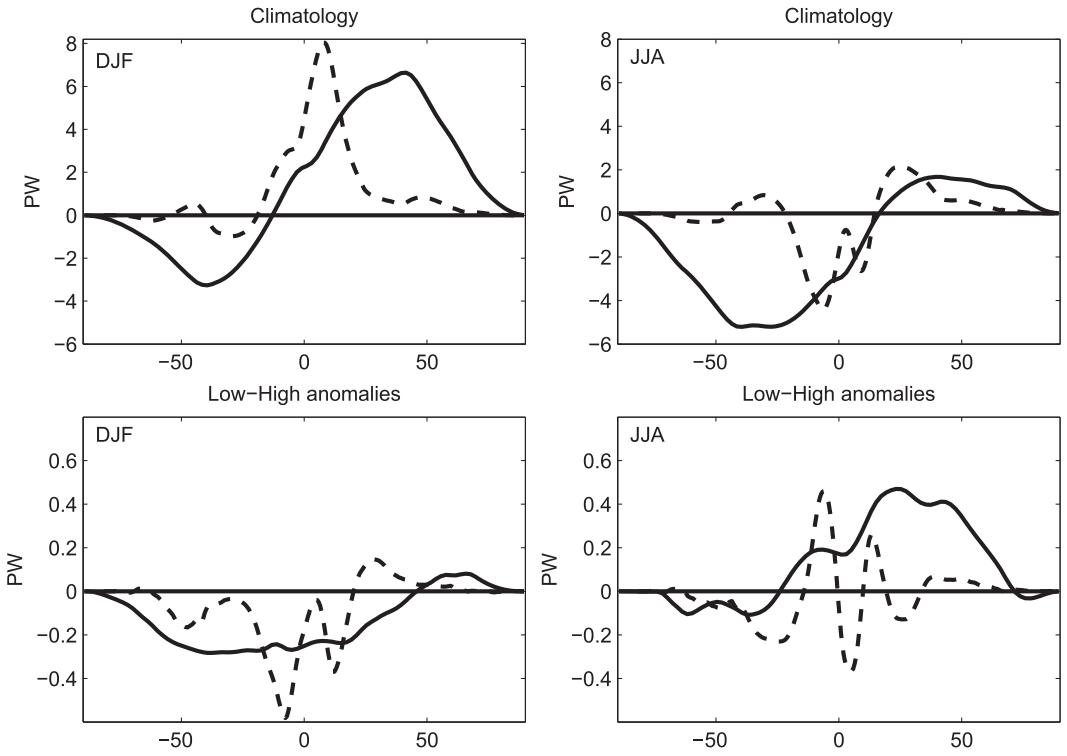

FIG. 5. Seasonal mean (DJF and JJA) atmospheric (solid lines) and ocean (dashed lines) meridional heat transport (PW) for (top) climatology and (bottom) low minus high obliquity conditions; (left) DJF and (right) JJA seasonal means. Ocean heat transport is calculated from ocean data. The atmospheric heat transport is calculated from monthly mean values of TOA and surface fluxes and including tendency terms. Also, a constant has been added to ensure zero heat transport at the poles.

In Eq. (1), ρ represents the density, c_p the heat capacity at constant pressure, z the depth, and T the temperature of the ocean. Also, SW_{surf} represents the net shortwave radiation, LW_{surf} the net longwave radiation, LH the latent heat, and SH the sensible heat at the ocean surface. It should be noted that in our analysis $\nabla \cdot F_o$ is calculated as the difference between the storage term and Q_{NET}. Under climatological conditions in midlatitudes $\nabla \cdot F_o$ is modest (Fig. 6, top). This means that in local summer, the midlatitudes ocean stores almost all the heat it receives from the atmosphere (positive Q_{NET}); in local winter it releases the thermal energy to the atmosphere (negative Q_{NET}). In contrast, in the tropics the heat exchange between the ocean and the atmosphere is smaller compared to higher latitudes. This means that a large portion of the heat stored is balanced by oceanic heat transport. As obliquity becomes smaller, the reduced surface heating of the ocean by the atmosphere ($\Delta Q_{NET} < 0$) at high and middle latitudes of the summer hemisphere is almost entirely balanced by a reduction in the storage term, as changes in $\nabla \cdot F_o$ are small (Fig. 6, bottom). On the other hand, in the winter hemisphere, the increased heat flux from the atmosphere to the ocean is almost entirely balanced by increasing ocean heat storage. Within the tropics, changes in Q_{NET} are small, which means that the large changes in storage term must be balanced by almost comparable anomalies of $\nabla \cdot F_o$ (heat transport). These results underscore the importance of ocean dynamics and thermodynamics in balancing part of the forcing.

d. *Circulation on dry and moist isentropes*

Although the zonal mean Eulerian streamfunction adequately depicts the meridional overturning circulation and its changes in the tropics, it may not be as useful for interpreting the midlatitude circulation in which eddy activity dominates (Pauluis et al. 2010). Midlatitude eddies connect the tropics with the high latitudes and are responsible for transporting most of the moisture, heat, and momentum poleward (Laliberté et al. 2012). The use of isentropic surfaces as a vertical coordinate system more accurately captures the meridional trajectories of individual parcels. For a more detailed description of the climatology of the isentropic circulation, see Pauluis et al. (2010) and Laliberté et al. (2012). The calculation of the circulation on dry and moist isentropes (e.g., Fig. 7) performed here follow the approach of Laliberté et al. (2012):

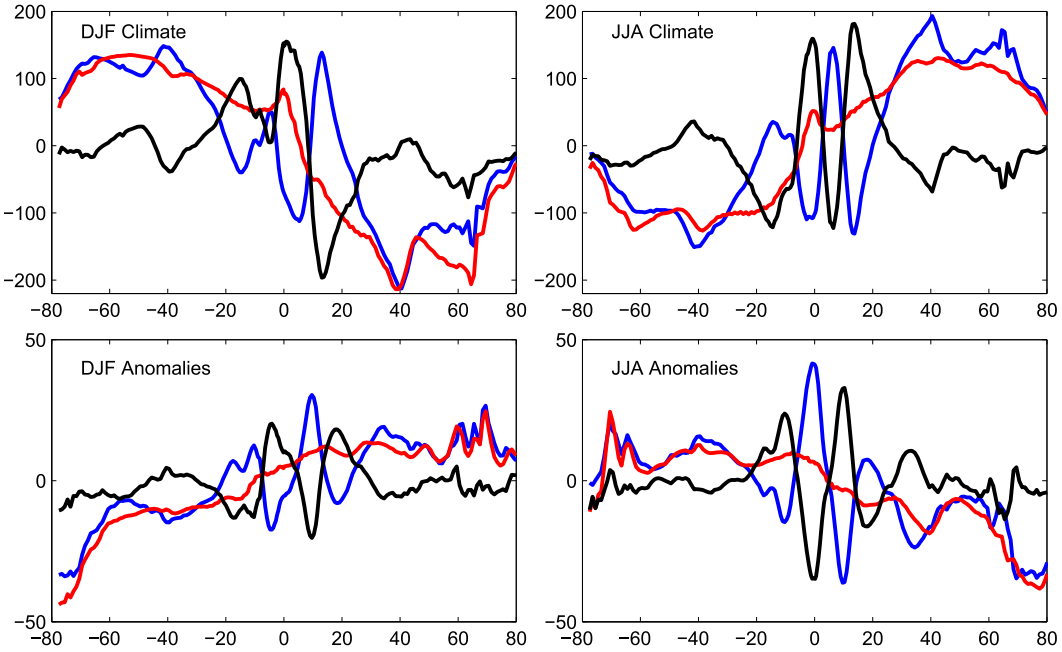

FIG. 6. (top) Climatological conditions and (bottom) anomalies (low minus high) in (left) DJF and (right) JJA for Q_{NET} (red), heat storage (blue) and $\nabla \cdot F_o$ (black); $\nabla \cdot F_o$ has been calculated as the difference of the former two. (Units are W m^{-2}.)

$$\Psi_{\theta}(\phi,\tilde{\theta}) = \frac{2\pi a\cos\phi}{g}\left[\int_0^{p_s} vH(\theta-\tilde{\theta})\,dp\right] \quad \text{and}$$

$$\Psi_{\theta_e}(\phi,\tilde{\theta}_e) = \frac{2\pi a\cos\phi}{g}\left[\int_0^{p} vH(\theta_e-\tilde{\theta}_e)\,dp\right], \qquad (2)$$

where H is the Heaviside function, p_s is the surface pressure, and θ and θ_e represent the potential and the equivalent potential temperatures, respectively. Unlike the mean Eulerian streamfunction, both the dry and moist isentropic circulations are characterized by single overturning cells in the winter hemisphere that seamlessly connects the low and high latitudes. The circulation on dry isentropes exhibits two local maxima: one in the tropics, corresponding to the Hadley circulation, and one in the midlatitudes in the vicinity of strongest baroclinic activity. In contrast, the circulation on moist isentropes is represented by a single cell that maximizes in the midlatitudes and spans the entire hemisphere. The circulation on moist isentropes is stronger than the circulation on dry isentropes, with the difference associated with the poleward flow of moist air rising from the surface to the upper troposphere in the midlatitudes (Pauluis et al. 2008). It should be noted here that the simulated maximum of Ψ_{θ_e} is located in the tropics and not in the midlatitudes, as in reanalysis data (Pauluis et al. 2011). This bias may be associated with underestimation of winter eddy activity in the GFDL model. In the summer hemisphere, the primary focus below, the isentropic circulation is much weaker.

The largest anomalies in both the dry and moist isentropic circulations occur in the summer hemisphere and the tropics, consistent with the orbital forcing. Some of the changes evident in the Eulerian streamfunction also appear in the isentropic circulation, reflecting consistency among the results (e.g., the equatorward shift in the boundary of the winter Hadley cell and the weakening of the maximum of the streamfunction in the tropics). On the other hand, some other features depend on the vertical coordinate system. For instance, the DJF Ψ_{θ} in the Southern Hemisphere strengthens at low values of θ consistently across all latitudes. Moreover, Ψ_{θ} strengthens in JJA in the Northern Hemisphere, even though this circulation is not well defined in its climatology. On the other hand, Ψ_{θ_e} shows a shift toward lower equivalent potential temperature in the summer hemisphere, as a result of the cooling and drying at these latitudes. Embedded in this shift is an overall strengthening of the circulation on moist isentropes in the summer hemisphere [i.e., the maximum streamfunction increases by 26% in the Northern Hemisphere (JJA) and 6% in the Southern Hemisphere (DJF)].

To separate the effects of strengthening and lowering of the circulation, we apply the statistical transformed Eulerian mean (STEM), which is an approximation to

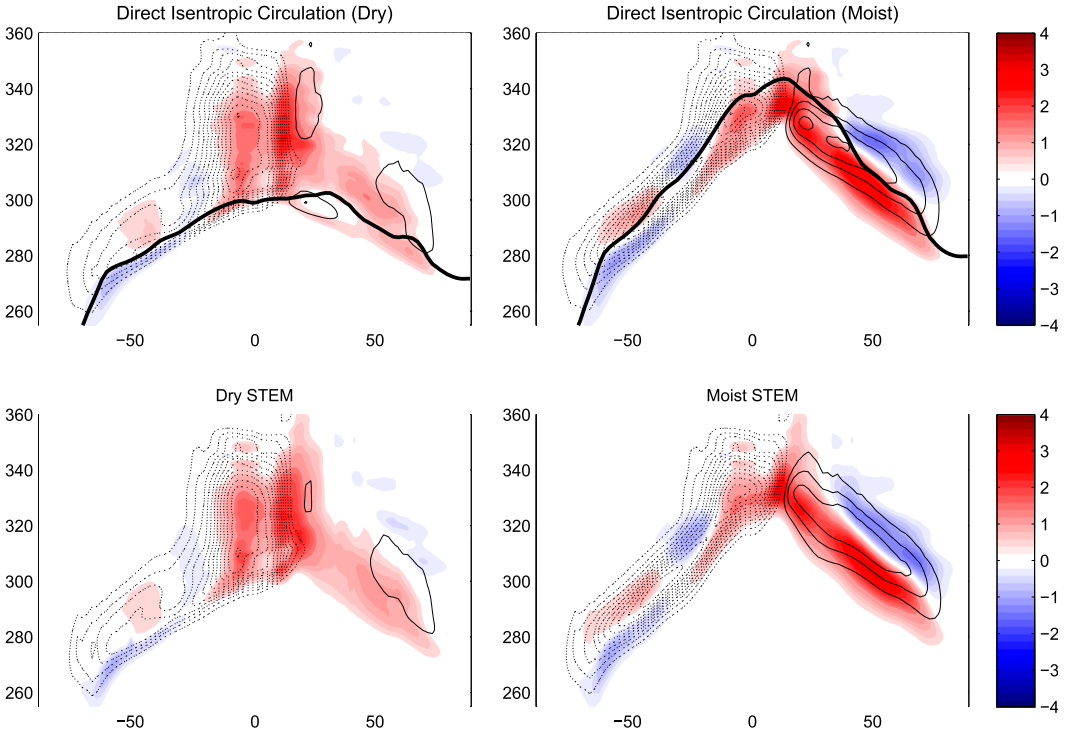

FIG. 7. Two methods of representing the JJA atmospheric meridional overturning circulation on isentropes ($kg\,s^{-1}$): (top) Direct computation of the meridional streamfunction on (left) dry and (right) moist isentropes, and (bottom) STEM streamfunction for (left) dry and (right) moist isentropes. Contours represent climatological conditions and colors represent low minus high anomalies. Thick lines represent potential temperature and equivalent potential temperatures at the surface.

the mean meridional circulation on dry and moist isentropes (Pauluis et al. 2011). The use of STEM offers several advantages over the exact isentropic circulation. First, its computation requires only monthly-mean zonal averages of meridional velocity $\overline{v}$, mean isentropes $\overline{\theta}$, meridional eddy transport $\overline{v'\theta'}$, and eddy variance $\overline{\theta'^2}$. Second, it can be decomposed into a mean Eulerian and an eddy components. Third, it can be applied to nonstratified coordinates like θ_e. The mean and eddy components of the STEM on dry isentropes are given by

$$\Psi_{\theta,\mathrm{mean}}(\phi,\overline{\theta}) = \int_{250\mathrm{K}}^{380\mathrm{K}}\int_0^{p_s} \frac{2\pi a\cos\phi}{\sqrt{2\pi g}}\frac{\overline{v}}{\overline{\theta'^2}^{1/2}} \exp\left[\frac{-(\tilde{\theta}-\overline{\theta})^2}{2\overline{\theta'^2}}\right] dp\, d\tilde{\theta} \quad \text{and}$$

$$\Psi_{\theta,\mathrm{eddy}}(\phi,\overline{\theta}) = \int_{250\mathrm{K}}^{380\mathrm{K}}\int_0^{p_s} \frac{2\pi a\cos\phi}{\sqrt{2\pi g}}\frac{\overline{v'\theta'}(\tilde{\theta}-\overline{\theta})}{\overline{\theta'^2}^{3/2}} \exp\left[\frac{-(\tilde{\theta}-\overline{\theta})^2}{2\overline{\theta'^2}}\right] dp\, d\tilde{\theta}. \quad (3)$$

The sum of $\Psi_{\theta,\mathrm{mean}}(\phi,\overline{\theta})$ and $\Psi_{\theta,\mathrm{eddy}}(\phi,\overline{\theta})$ is the STEM on dry isentropes. Analogously, STEM on moist isentropic surfaces is obtained by replacing θ with θ_e.

Comparing Figs. 7 and 8, the STEM computed on both dry and moist isentropic surfaces is seen to agree well with the exact isentropic circulation [computed from Eq. (3)] for both climatology and low minus high anomalies. In particular, the STEM captures the weakening of the Hadley circulation, the equatorward shift of its boundary, and the strengthening of the circulation on dry isentropes in the Northern Hemisphere during JJA. Additionally, the STEM on moist isentropes captures the shift of the summer circulation to lower equivalent potential temperature as well as its strengthening (18% during JJA and 6% during DJF).

Another advantage of using STEM is that it allows separation of the circulation anomalies of the mean Eulerian component into changes from the mean meridional velocity ($\Delta\overline{v}$), mean isentropes ($\Delta\overline{\theta}$ and $\Delta\overline{\theta_e}$), and their variances ($\Delta\overline{\theta'^2}$ and $\Delta\overline{\theta_e'^2}$) (Wu and Pauluis 2013). In a similar way, the circulation anomalies of the eddy component can be decomposed into effects from changing mean meridional eddy flux ($\Delta\overline{v'\theta'}$ and $\Delta\overline{v'\theta_e'}$), mean isentropes ($\Delta\overline{\theta}$ and $\Delta\overline{\theta_e}$), and their

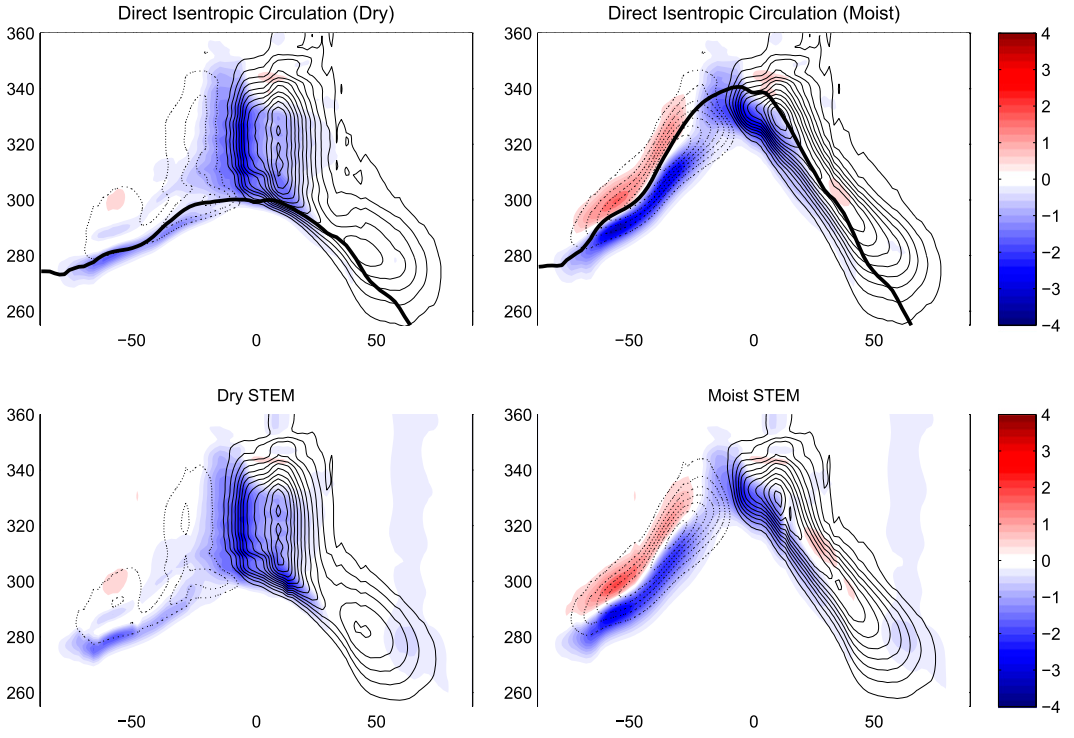

FIG. 8. As in Fig. 7, but for DJF.

variances ($\Delta\overline{\theta'^2}$ and $\Delta\overline{\theta_e'^2}$). Given that the changes in the isentropic circulation are qualitatively similar for both DJF and JJA, in the following we focus on JJA for simplicity. Also, changes in the mean and eddy components of STEM associated with changing variance of the mean isentropes ($\Delta\overline{\theta'^2}$ and $\Delta\overline{\theta_e'^2}$) are not plotted because they are small compared to the other two effects.

For the dry STEM, the changes in $\overline{\theta}$ correspond to an "upward" shift of the Hadley circulation toward warmer temperatures (Fig. 9e), which is consistent with obliquity-induced warming of the tropics. In contrast, in the midlatitudes the response of Ψ_θ to changes in $\overline{\theta}$ corresponds to a "downward" shift of the eddy circulation toward cooler temperatures (Fig. 9f) as a result of the obliquity-induced cooling of the whole troposphere (note the opposite sign in the streamfunction in midlatitudes). The Ψ_θ anomaly associated with weakening of the mean meridional velocity corresponds to weakening of the Hadley circulation and an equatorward shift in its boundary (Fig. 9c). Furthermore, the strengthening of the eddy circulation on dry isentropes confirms that the poleward eddy sensible heat flux $\overline{v'\theta'}$ increases (Fig. 9d), as a result of the increased equator-to-pole insolation gradient.

The decomposition of the moist STEM (Fig. 10) shares several similarities with the dry STEM. The larger upward shift of the circulation in the tropics and the larger downward shift in the midlatitudes are associated with moistening and drying accompanying increase and decrease in temperature, respectively. Furthermore, the increase in the eddy component of the moist isentropic circulation is strengthened beyond that in the dry isentropic circulation: this intensification arises since the moist isentropic circulation transports eddy latent as well as sensible heat flux, with the former increasing for low obliquity. The use of isentropic surfaces as a vertical coordinate system facilitates visualization of the overturning circulation not only in the tropics but over all latitudes. For example, the penetration of the circulation anomalies associated with midlatitude eddies deep into the tropics, at the same latitude where the shift in the boundary of the Hadley cell is located, hints that the two processes may be linked.

4. Summary and discussion

A reduction in Earth's obliquity alters the seasonal distribution of the TOA insolation, with the summer hemisphere becoming cooler and the winter hemisphere becoming warmer (with the exception of the high latitudes), thereby reducing the interhemispheric insolation contrast. The warm hemisphere additionally experiences a strengthening of the meridional insolation gradient. The latter is associated with a strengthening of the meridional temperature gradient in the subtropics

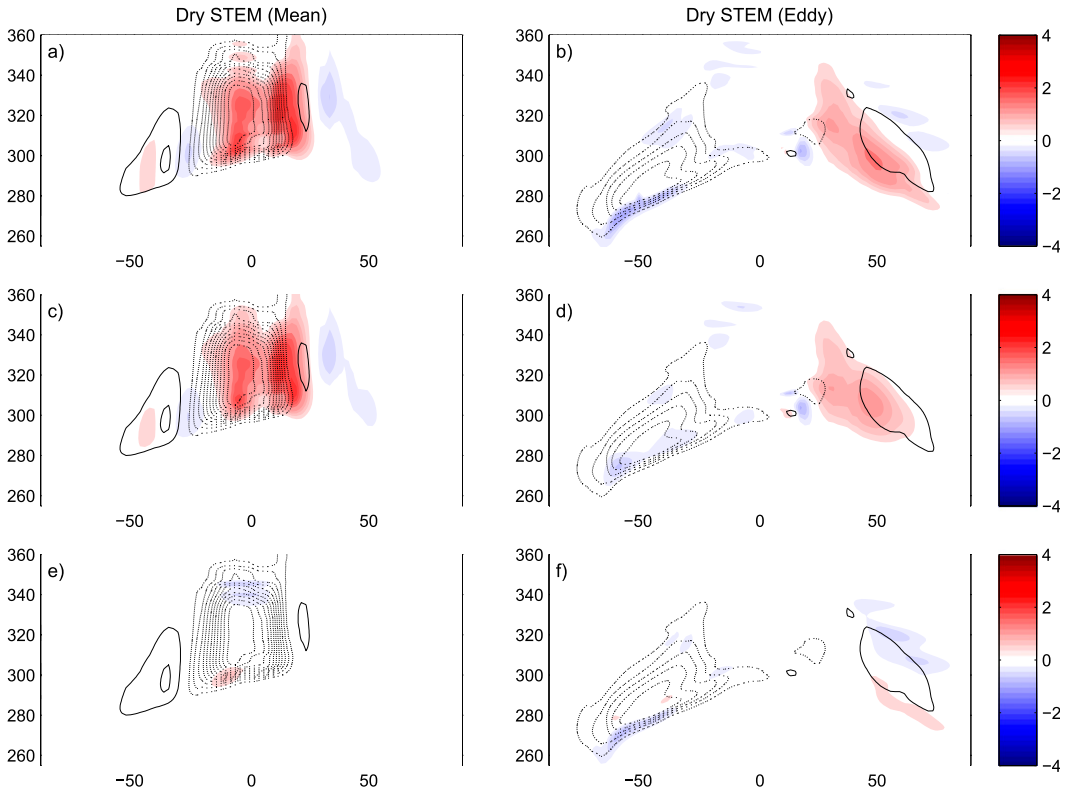

FIG. 9. Separation of the JJA dry STEM into Eulerian (a) mean and (b) eddy component. The mean component of STEM is further decomposed into contributions from (c) $\Delta\overline{v}$ and (e) $\Delta\overline{\theta}$. The eddy component of STEM is further decomposed into contributions from (d) $\Delta\overline{v'\theta'}$ and (f) $\Delta\overline{\theta}$. Contours represent climatological conditions and colors represent low minus high anomalies. (Units are kg s^{-1}.)

of the summer hemisphere, which causes the subtropical jet to expand equatorward. The change in the zonal jet is further accompanied by strengthening of the vertical wind shear, and as the static stability remains constant in the subtropics, this points to strengthening of the baroclinic instability. This is further confirmed by the increase in the midlatitude atmospheric heat transport, which is dominated by baroclinic eddies. In contrast, the Hadley circulation weakens as a response to the weaker interhemispheric insolation contrast. This is reflected in the weakening of the winter Hadley circulation as well as the diminished cross-equatorial heat transport. Within the tropics the insolation forcing is partly balanced by a weakening of the cross-equatorial ocean heat transport, which manifests a comparable contribution to the net transport as the atmosphere during DJF but a considerably smaller contribution during JJA. The dominant winter Hadley cell also experiences an equatorward displacement of its ascending branch and associated ITCZ. This results in an equatorward expansion of the eddy-driven summer cell, although its poleward edge also moves toward the equator. See Fig. 11 for an illustration of the key components of the atmospheric circulation changes induced by the change in obliquity.

The weakening of the Hadley cell, the equatorward retreat of its ascending branch, and the increase in the static stability in the tropics exhibit some apparent resemblance to the changes evident in twenty-first-century global warming simulations of the Special Report on Emissions Scenarios' A2 high emission scenario, where CO_2 concentrations reach 800 ppm at the end of the twenty-first century (Held and Soden 2006; Lu et al. 2008), although the mechanisms may not be analogous. In the global warming scenario studies, strengthening of the dry static stability, associated with the increase in boundary layer moisture following the temperature increase according to Clausius–Clapeyron, outpaces the increase in diabatic heating, so the tropical overturning circulation weakens. In our obliquity experiments the weakening of the Hadley circulation is roughly 25% of the weakening simulated by the A2 scenario of the global warming experiments. However, the increase of dry static stability as well as temperature in the tropics in our case is an order of magnitude weaker than in the global warming case. On the other hand, the magnitude

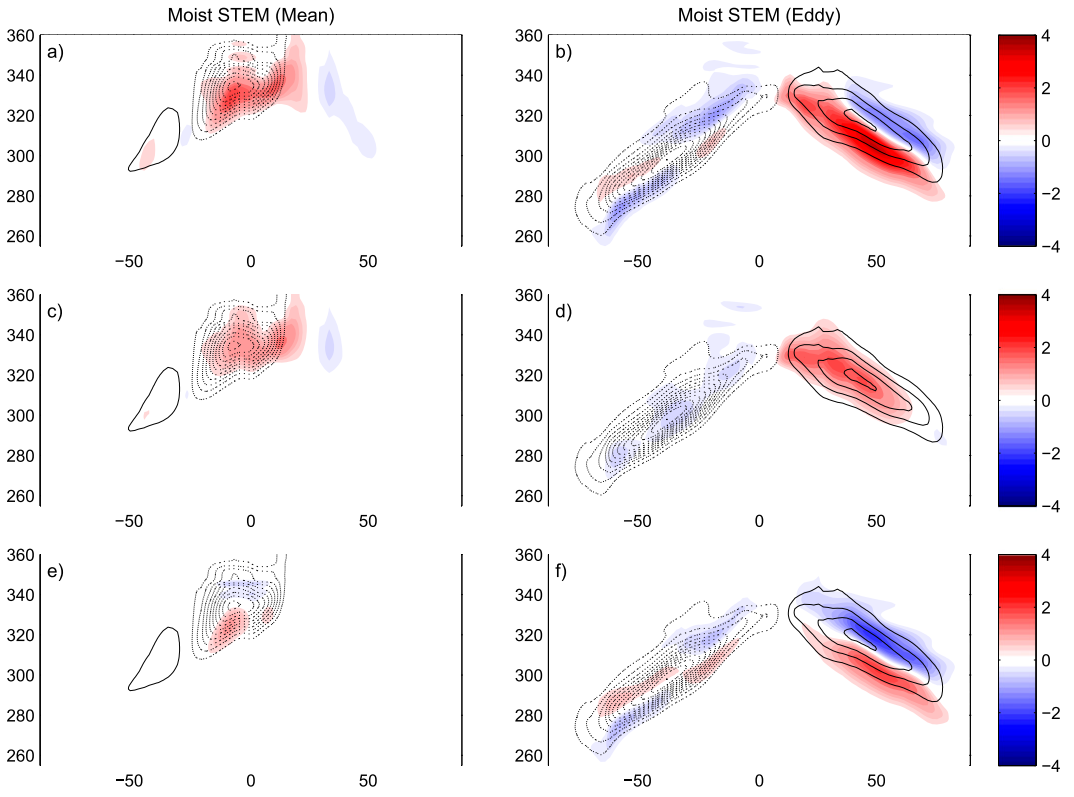

FIG. 10. As in Fig. 9, but for moist STEM.

of the shift of the Hadley cell boundary is roughly twice as large compared to the global warming case. These finding suggest that the change in the Hadley circulation simulated by the obliquity experiments does not share the same thermodynamic explanation as the one implicated in the global warming case. The most likely explanation is that in our case the equatorward shift in the Hadley cell boundary (which had the opposite sign in the global warming case) overwhelms any other tropical thermodynamic processes that might influence how the Hadley cell behaves. Furthermore, under obliquity forcing the SST response is very weak compared to the global warming case, where the tropics warm by several degrees, which can also partly explain the difference in the Hadley response between the two cases.

However, our findings have some qualitative similarities with those of global warming regarding the summer hemisphere Hadley cell, which is driven by baroclinic eddies (Walker and Schneider 2006; Lu et al. 2008; Kang and Lu 2012). Under global warming the summer Hadley cell expands poleward as the baroclinic instability weakens (Lu et al. 2008). For low minus high obliquity, the subtropical baroclinic eddies strengthen and the summer Hadley cell contracts equatorward. Even though the changes in the baroclinic activity appear to arise from distinct causes (the global warming studies implicate strengthening of static stability with wind shear playing a secondary role, which is opposite to the obliquity forcing) the apparent resemblance of the link between baroclinic activity and summer cell geometry suggests a common underlying mechanism. This mechanism is based on the fact that as the midlatitude eddy activity weakens the eddy-driven summer cell can reach farther poleward before it becomes baroclinically unstable (Kang and Lu 2012).

The forcing associated with a change in Earth's obliquity also has qualitative similarities with that of ENSO heating, which is located on the equator (Lu et al. 2008; note that their study focuses on DJF seasonal means). More specifically, the tropics warm as in the ENSO case, even though it is much weaker and is slightly asymmetric with respect to the equator. The response to equatorial ENSO heating induces an increase in the subtropical temperature gradient and an equatorial displacement of the eddy-driven jet (Lu et al. 2008), exactly as in the obliquity case. The result for the ENSO case is an increase in baroclinic instability at those latitudes. In both the ENSO as well as the obliquity case the increase in baroclinicity is attributed to an increase in the vertical shear, with the change in static stability having a smaller

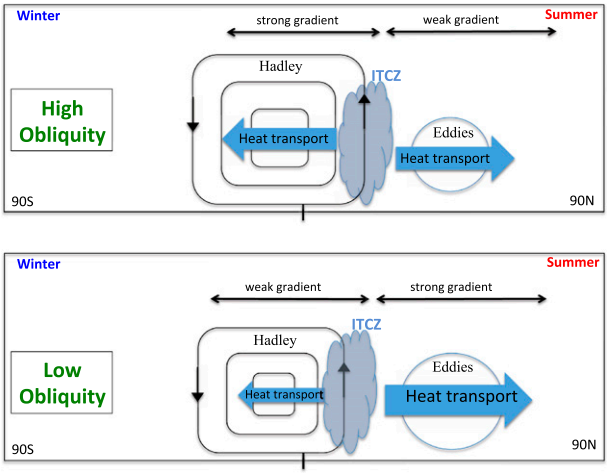

FIG. 11. Schematic representation of the circulation changes associated with a change in obliquity during boreal summer (JJA). Arrows represent heat transport, with direction indicating sign and the size of the arrows representing relative magnitude.

impact. Additionally, in both cases the ITCZ, which defines the boundary between the dominant winter cell and the weak summer cell, shifts in the same direction with the poleward edge of the summer cell. A similar relationship between the ITCZ and the eddy-driven summer cell was found by Kang and Lu (2012) in global warming scenarios. Therefore, our findings underscore the close connection between the ITCZ and midlatitude eddies.

Acknowledgments. We thank Olivier Pauluis and Tiffany Shaw for useful discussion and Frederic Laliberté for assistance with isentropic streamfunction calculations. This work was supported by a National Science Foundation (NSF) Paleoclimate Perspectives on Climate Change Initiative Grant AGS-1103209.

REFERENCES

Berger, A., and M. F. Loutre, 1991: Insolation values for the climate of the last 10 million years. *Quat. Sci. Rev.,* **10,** 297–317, doi:10.1016/0277-3791(91)90033-Q.

Bordoni, S., and T. Schneider, 2010: Regime transitions of steady and time-dependent Hadley circulations: Comparison of axisymmetric and eddy-permitting simulations. *J. Atmos. Sci.,* **67,** 1643–1654, doi:10.1175/2009JAS3294.1.

Broccoli, A. J., K. A. Dahl, and R. J. Stouffer, 2006: Response of the ITCZ to Northern Hemisphere cooling. *Geophys. Res. Lett.,* **33,** L01702, doi:10.1029/2005GL024546.

Chiang, J. C. H., and C. M. Bitz, 2005: Influence of high latitude ice cover on the marine intertropical convergence zone. *Climate Dyn.,* **25,** 477–496, doi:10.1007/s00382-005-0040-5.

Delworth, T. L., and Coauthors, 2006: GFDL's CM2 global coupled climate models. Part I: Formulation and simulation characteristics. *J. Climate,* **19,** 643–674, doi:10.1175/JCLI3629.1.

Dima, I. M., and J. M. Wallace, 2003: On the seasonality of the Hadley cell. *J. Atmos. Sci.,* **60,** 1522–1527, doi:10.1175/1520-0469(2003)060<1522:OTSOTH>2.0.CO;2.

Erb, M. P., A. J. Broccoli, and A. C. Clement, 2013: The contribution of radiative feedbacks to orbitally driven climate change. *J. Climate,* **26,** 5897–5914, doi:10.1175/JCLI-D-12-00419.1.

Held, I. M., 2000: The partitioning of the poleward energy transport between the tropical ocean and atmosphere. *J. Climate,* **58,** 943–948, doi:10.1175/1520-0469(2001)058<0943:TPOTPE>2.0.CO;2.

——, and A. Y. Hou, 1980: Nonlinear axially symmetric circulations in a nearly inviscid atmosphere. *J. Atmos. Sci.,* **37,** 515–533, doi:10.1175/1520-0469(1980)037<0515:NASCIA>2.0.CO;2.

——, and T. Schneider, 1999: The surface branch of the zonally averaged mass transport circulation in the troposphere. *J. Atmos. Sci.,* **56,** 1688–1697, doi:10.1175/1520-0469(1999)056<1688:TSBOTZ>2.0.CO;2.

——, and B. J. Soden, 2006: Robust responses of the hydrological cycle to global warming. *J. Climate,* **19,** 5686–5699, doi:10.1175/JCLI3990.1.

Hewitt, C. D., and J. F. B. Mitchell, 1998: A fully coupled GCM simulation of the climate of the mid-Holocene. *Geophys. Res. Lett.,* **25,** 361–364, doi:10.1029/97GL03721.

Kang, S. M., and J. Lu, 2012: Expansion of the Hadley cell under global warming: Winter versus summer. *J. Climate,* **25,** 8387–8393, doi:10.1175/JCLI-D-12-00323.1.

——, I. M. Held, D. M. W. Frierson, and M. Zhao, 2008: The response of the ITCZ to extratropical thermal forcing: Idealized slab-ocean experiments with a GCM. *J. Climate,* **21,** 3521–3532, doi:10.1175/2007JCLI2146.1.

Laliberté, F., T. Shaw, and O. Pauluis, 2012: Moist recirculation and water vapor transport on dry isentropes. *J. Atmos. Sci.,* **69,** 875–890, doi:10.1175/JAS-D-11-0124.1.

Lawrence, K. T., Z. Liu, and T. D. Herbert, 2006: Evolution of the eastern tropical Pacific through Plio-Pleistocene glaciation. *Science,* **312,** 79–83, doi:10.1126/science.1120395.

Liu, Z., and T. D. Herbert, 2004: High-latitude influence on the eastern equatorial Pacific climate in the early Pleistocene epoch. *Nature,* **427,** 720–723, doi:10.1038/nature02338.

Lu, J., G. Chen, and D. M. W. Frierson, 2008: Response of the zonal mean atmospheric circulation to El Niño versus global warming. *J. Climate,* **21,** 5835–5851, doi:10.1175/2008JCLI2200.1.

Mantsis, D. F., and A. C. Clement, 2009: Simulated variability in the mean meridional atmospheric circulation over the 20th century. *Geophys. Res. Lett.,* **36,** L06704, doi:10.1029/2008GL036741.

——, ——, A. J. Broccoli, and M. P. Erb, 2011: Climate feedbacks in response to changes in obliquity. *J. Climate,* **24,** 2830–2845, doi:10.1175/2010JCLI3986.1.

Pauluis, O., A. Czaja, and R. Korty, 2008: The global atmospheric circulation on moist isentropes. *Science,* **321,** 1075–1078, doi:10.1126/science.1159649.

——, ——, and ——, 2010: The global atmospheric circulation in moist isentropic coordinates. *J. Climate,* **23,** 3077–3093, doi:10.1175/2009JCLI2789.1.

——, T. Shaw, and F. Laliberté, 2011: A statistical generalization of the transformed Eulerian-mean circulation for an arbitrary vertical coordinate system. *J. Atmos. Sci.,* **68,** 1766–1783, doi:10.1175/2011JAS3711.1.

Phillips, N. A., 1954: Energy transformations and meridional circulations associated with simple baroclinic waves in a

two-level, quasi-geostrophic model. *Tellus,* **6,** 273–286, doi:10.1111/j.2153-3490.1954.tb01123.x.

Raymo, E. M., and K. Nisancioglu, 2003: The 41 kyr world: Milankovitch's other unsolved mystery. *Paleoceanography,* **18,** 1011, doi:10.1029/2002PA000791.

Schneider, T., 2006: The general circulation of the atmosphere. *Annu. Rev. Earth Planet. Sci.,* **34,** 655–688, doi:10.1146/annurev.earth.34.031405.125144.

——, and S. Bordoni, 2008: Eddy-mediated regime transitions in the seasonal cycle of a Hadley circulation and implications for monsoon dynamics. *J. Atmos. Sci.,* **65,** 915–934, doi:10.1175/2007JAS2415.1.

Simmonds, I., and E.-P. Lim, 2009: Biases in the calculation of Southern Hemisphere mean baroclinic eddy growth rate. *Geophys. Res. Lett.,* **36,** L01707, doi:10.1029/2008GL036320.

Trenberth, K. E., and J. M. Caron, 2001: Estimates of meridional atmosphere and ocean heat transports. *J. Climate,* **14,** 3433–3443, doi:10.1175/1520-0442(2001)014<3433:EOMAAO>2.0.CO;2.

Vimeux, F., V. Masson, J. Jouzel, M. Stievenard, and J. R. Petit, 1999: Glacial–interglacial changes in the ocean surface conditions in the Southern Hemisphere. *Nature,* **398,** 410–413, doi:10.1038/18860.

Walker, C. C., and T. Schneider, 2006: Eddy influences on Hadley circulations: Simulations with an idealized GCM. *J. Atmos. Sci.,* **63,** 3333–3350, doi:10.1175/JAS3821.1.

Wu, Y., and O. Pauluis, 2013: Examination of isentropic circulation response to a doubling of carbon dioxide using a statistical transformed Eulerian mean streamfunction. *J. Atmos. Sci.,* **70,** 1649–1667, doi:10.1175/JAS-D-12-0235.1.

Yoshimori, M., and A. J. Broccoli, 2008: Equilibrium response of an atmosphere-mixed layer ocean model to different radiative forcing agents: Global and zonal mean response. *J. Climate,* **21,** 4399–4423, doi:10.1175/2008JCLI2172.1.

Zhang, R., and T. L. Delworth, 2005: Simulated tropical response to a substantial weakening of the Atlantic thermohaline circulation. *J. Climate,* **18,** 1853–1860, doi:10.1175/JCLI3460.1.